NANO LETTERS

Letter

pubs.acs.org/NanoLett

Controlling the Electrical Transport Properties of Nanocontacts to Nanowires

Alex M. Lord,[†] Thierry G. Maffeis,[‡] Olga Kryvchenkova,[‡] Richard J. Cobley,[‡] Karol Kalna,[§] Despoina M. Kepaptsoglou,[⊥] Quentin M. Ramasse,[⊥] Alex S. Walton,[#] Michael B. Ward,[%] Jürgen Köble,[&] and Steve P. Wilks*[,∥]

[†]Centre for NanoHealth, College of Engineering, [‡]Multidisciplinary Nanotechnology Centre, College of Engineering, [§]Electronic Systems Design Centre, College of Engineering, and [∥]Multidisciplinary Nanotechnology Centre, Department of Physics, College of Science, University of Swansea, Singleton Park SA2 8PP, United Kingdom

[⊥]SuperSTEM Laboratory, SFTC Daresbury Campus, Keckwick Lane, Daresbury WA4 4AD, United Kingdom

[#]School of Physics and Astronomy and [%]Institute for Materials Research, University of Leeds, Leeds LS2 9JT, United Kingdom

[&]Omicron Nanotechnology GmbH, Limburger Straße 75, 65232 Taunusstein, Germany

S *Supporting Information*

ABSTRACT: The ability to control the properties of electrical contacts to nanostructures is essential to realize operational nanodevices. Here, we show that the electrical behavior of the nanocontacts between free-standing ZnO nanowires and the catalytic Au particle used for their growth can switch from Schottky to Ohmic depending on the size of the Au particles in relation to the cross-sectional width of the ZnO nanowires. We observe a distinct Schottky to Ohmic transition in transport behavior at an Au to nanowire diameter ratio of 0.6. The current−voltage electrical measurements performed with a multiprobe instrument are explained using 3-D self-consistent electrostatic and transport simulations revealing that tunneling at the contact edge is the dominant carrier transport mechanism for these nanoscale contacts. The results are applicable to other nanowire materials such as Si, GaAs, and InAs when the effects of surface charge and contact size are considered.

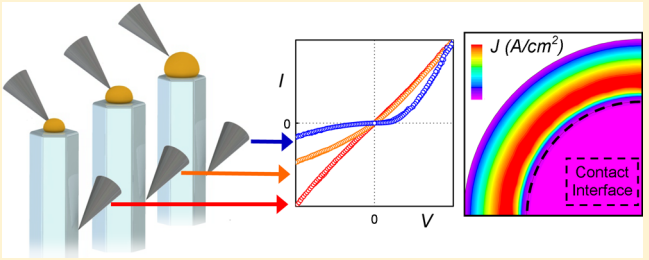

KEYWORDS: *Electrical contacts, nanowires, edge effect, tunneling, Ohmic, Schottky*

In metal−semiconductor contacts, the electrical conductivity is determined by the intrinsic properties of the materials and the interface they form.[1−4] At the microscale, the size of the contact has little effect on the transport mechanisms. However, at the nanoscale, dipole-like electrostatic fields replace uniform parallel fields leading to electrical behavior that is not fully understood.[5] Indeed, some prototype devices using nanomaterials such as lasers[6] and nanogenerators[7] have been demonstrated in laboratories, but the difficulty in selecting Ohmic- or Schottky-like contacts[5,8] makes repeatable manufacture challenging.

Experimental evidence of Schottky- or Ohmic-like behavior has been observed for size-selected metal clusters deposited onto large planar semiconductor surfaces.[4,9−11] Other works measuring contacts on the tips of free-standing semiconductor nanowires have also shown a range of rectifying or Ohmic behavior for different metals deposited onto ZnO nanowires.[12,13] Furthermore, Au catalyst particles, used to grow a multitude of nanowires, have demonstrated Ohmic behavior[14] for InAs and InP as-grown nanowires, yet rectifying behavior on Ge nanowires.[15] Léonard et al. reported declining contact rectification for Ge nanowire diameters less than 60 nm. While it is clear there is a range of electrical behavior possible for nanoscale metal contacts, there is no generalized understanding of how the transport properties are determined by the size of the metal contact in relation to the nanowire geometry.[11,15−17] In this work, we investigate the effect of contact size on nanoscale electron transport as a function of contact and nanowire diameter using an innovative multiprobe experimental protocol in combination with full 3D simulations.

A multiprobe experimental system was used to study the behavior of nanocontacts on free-standing ZnO nanowires,[13,18] grown using Au catalyst particles that provide an intrinsic metal contact to the tip of the vertically orientated nanostructures. The current−voltage (I−V) measurements reveal a spectrum of electrical behavior from Schottky-like to Ohmic-like. This transition in transport behavior is not directly dependent on the size of the nanowire (or the Au particle), but instead it is correlated to the size of the contact in relation to the nanowire diameter. Specifically we found that the transition from

Received: September 29, 2014
Revised: May 28, 2015
Published: June 4, 2015

DOI: 10.1021/nl503743t
Nano Lett. 2015, 15, 4248−4254

Schottky-like to Ohmic-like happens when the Au contact to nanowire diameter ratio decreases below 0.6. To explain the observed change in the rectifying characteristics, full 3D numerical simulations were necessary to reveal the features of the depletion region that allowed the enhanced transport in the nanoscale contacts. Our findings show that the quantum-mechanical tunneling of electrons through the depletion region at the contact edge is the main transport mechanism and provides the capability to control the conductivity of metal–nanowire interfaces. By comparing the metal contact at the tip of a nanowire in relation to the nanowire diameter, it is possible to "turn on" or "turn off" the effects of edge tunneling, which is of paramount importance to many recent and previous results.[4,5,14−16,19−21] The main conclusion from the work is that the conductivity is not just determined by contact size but also crucially by the size of the interface in relation to the nanowire diameter. In addition, the simulations show the polarity of the charge on the nanowire surface can have an overriding effect on the contact transport properties for all nanowire materials.

Experimental Procedure. ZnO nanowires of diameters ranging from 20 to 120 nm were fabricated by chemical vapor deposition using Au catalyst particles to initiate their vertical growth on α-Al_2O_3 substrate. The vapor-phase nanowires were grown using a solid ZnO and C source evaporated in a controlled atmosphere in a tube furnace.[22] A thin layer (~5 nm) of Au was deposited on the substrate to initiate growth at ~900 °C with a flow of 49 sccm Ar and 1 sccm O_2 at 30 mbar chamber pressure.

After the growth, close inspection of the nanowires was initially performed using backscattered electron (BSE) imaging with a Hitachi S4800 scanning electron microscope (SEM) and transmission (TEM) electron microscopy. Samples were prepared for TEM analysis (FEI Tecnai TF20 FEGTEM operated at 200 keV) by rubbing a carbon support film (holey carbon film on 400 mesh Cu, Agar Scientific) across the top of the nanowire array. High-resolution high angle annular dark field (HAADF) imaging was carried out with a Nion UltraSTEM100 scanning transmission electron microscope (STEM) operated at 100 keV primary beam energy. The probe-forming optics, corrected for aberrations up to fifth order, were configured to provide ~100 pA of beam current with a 31 mrad beam convergence semiangle, for an estimated probe size of 0.8 Å. The inner and outer radii of the HAADF detector were calibrated at 79 and 195 mrad, respectively.

Accurately measuring the electrical properties of contacts to individual free-standing nanowires requires the use of more than one probe[13,18] to overcome the limitations of single-probe techniques such as AFM and STM. Here, the multiprobe technique was employed using an ultrahigh-vacuum Omicron LT nanoprobe with four independent tungsten probes guided by an *in situ* Gemini SEM column to measure the unmodified vertical array of ZnO nanowires at room temperature. The measurement technique used two scanning probes that were annealed in the ultrahigh-vacuum system,[23,24] one forming an Ohmic contact to the side of an individual nanowire while the other probe was placed in contact with the Au particle on the uppermost nanowire tip. This enabled a single Au–ZnO contact to be isolated in the as-grown configuration, providing a measurement of the metal–nanowire interface. The technique ensures accurate measurements that are free from any extraneous affects associated with the substrate or nanowire substrate junction.[18] A complete description of the measurement process is included in Supporting Information Figure S1.

Experimental Results. The initial electron microscopy of the nanowire array performed with BSE imaging (Figure 1a)

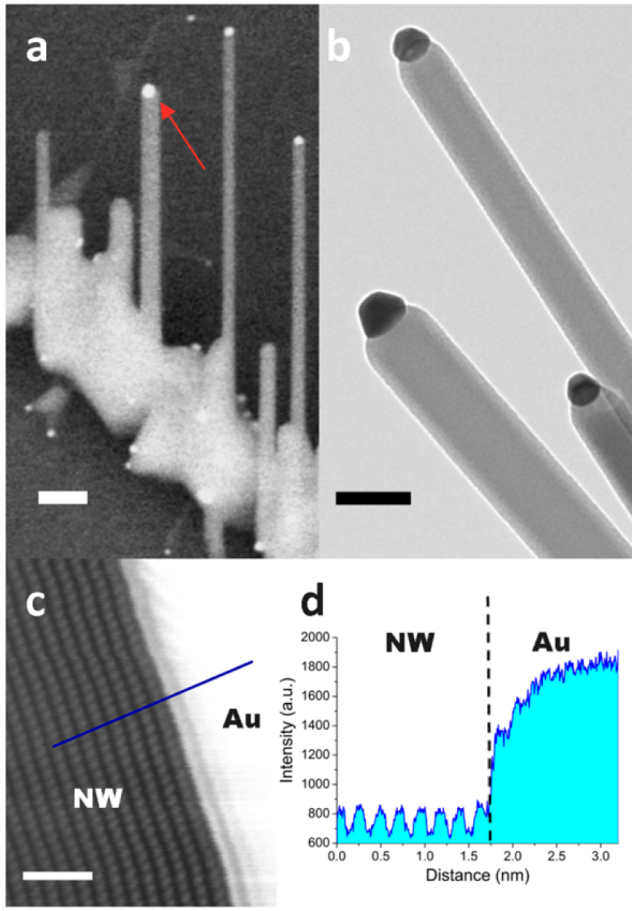

Figure 1. Electron microscopy images of ZnO nanowires and the Au catalyst particle interface. (a) BSE image showing the as-grown nanowire sample with a Au catalyst particle clearly visible at the nanowire tip; scale 200 nm. The red arrow indicates a 59 nm contact measured with the local multiprobe technique. (b) TEM image of several ZnO nanowires with a variation in the Au catalyst particle size that has no direct correlation with nanowire diameter; scale 30 nm. (c) Unprocessed aberration-corrected HAADF image of the Au–ZnO nanowire interface with the beam aligned along the $[01\bar{1}0]$ ZnO zone axis showing the abrupt interface, scale 1 nm. (d) Line profile of the interface corresponding to the blue line in (c) showing the expected equal intensity of Zn columns, with the intensity increase at the interface indicating an abrupt interface and no interfacial layer. The first Au column appears less intense due to the Au particle curvature.

showed distinct Au particles residing on the tips of the vertically free-standing ZnO nanowires. On closer inspection with TEM it was revealed that for similar size nanowires there was a variation in metal particle size independent of nanowire diameter (Figure 1b). This particular nanowire growth method can lead to contamination of the nanowire by the catalyst atoms,[25−27] producing a variability in electrical behavior[1,27] if present. This effect on the bulk properties can be discounted as the Au-catalyzed growth of ZnO exhibits no alloying due to the low solubility of the solid catalyst material in the nanowire during and after growth.[28−30] However, the structural and chemical integrity of the metal–nanowire interface plays a key

DOI: 10.1021/nl503743t
Nano Lett. 2015, 15, 4248−4254

role in its transport properties.[1−4,27,31] Hence, it was necessary to thoroughly investigate the nature and quality of the Au−ZnO nanowire junction. To investigate anomalies on the atomic level, interface images (Figure 1c) and corresponding line profiles (Figure 1d) were recorded using an aberration-corrected Nion UltraSTEM microscope with a probe size of 0.8 Å and HAADF detector. This revealed the periodic atomic Zn columns and an abrupt junction as indicated by the clear discontinuity in contrast on either side of the material interface. The Au−ZnO interface always appeared to be atomically flat, within the limits of electron microscopy (see Supporting Information Figure S2), with the nanowires orientated along [0001] such that the Au particle resided on the (0001) top facet. Using the HAADF technique, no Au atoms, compositional variation, or defects were detected in the nanowire material near the interface (for a detailed explanation of the HAADF technique, refer to Supporting Information Figures S2 and S3). The structural investigations showed the Au−ZnO nanowire interface is clean, flat, ordered, and intimate—an ideal test bed to develop a fundamental understanding of the intrinsic electrical properties of particle−nanowire contacts.

I−*V* measurements were recorded for 11 nanowires with diameters between 40 and 107 nm having a variety of Au contact size diameters between 23 and 71 nm. The measurement setup is depicted schematically in Figure 2, along with

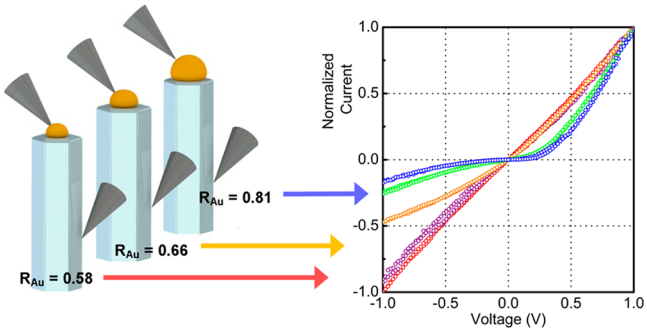

Figure 2. Experimental *I*−*V* measurements of Au contacts that provide R_{Au} of 0.55 (purple), 0.58 (red), 0.66 (orange), 0.71 (green), and 0.81 (blue) depicted by the schematic diagrams. The current is normalized to the value at +1 V for each nanowire (~0.5 μA). The absolute *I*−*V* curves are shown in the Supporting Information Figure S4.

typical measurements for five Au−ZnO nanowire contacts. The voltage triangulation, −1 to 1 V and 1 to −1 V, showed no hysteresis for each measurement, indicating that the interfaces were stable and unaffected by the high current densities. The measurements shown in Figure 2 were performed on Au particles of diameter 40, 23, 71, 50, and 44 nm supported on wires of 73, 40, 107, 70, and 54 nm, respectively. To enable direct comparison of the results, we define a parameter for nanosized contacts R_{Au} as the ratio of Au particle diameter to nanowire diameter, yielding R_{Au} values of 0.55, 0.58, 0.66, 0.71, and 0.81, for the nanowires in Figure 2. The results clearly show a transition from Ohmic-like to Schottky-like transport behavior as R_{Au} increases. The measured data are scaled to the value of the current at +1 V for each nanowire to illustrate the change in *I*−*V* shape; note that scaling has little effect on the curve shape as the absolute *I*−*V* data (see Supporting Information Figure S4) show similar current values for the five nanowires, particularly at +1 V. This shows that the change from Ohmic-like to Schottky-like behavior is not heavily influenced by series resistance. Series resistance originates from the side probe contact, the nanowire, and the measurement system (~100 ohm for the multiprobe instrument). If the series resistance is large in comparison with the Au−ZnO interface resistance, the true diode behavior of the contact can be masked. It is possible to estimate the series resistance from the *I*−*V* data in the bias region above the Schottky barrier (0.6 V) using the gradient near +1 V for the curves shown in Supporting Information Figure S4. For the five nanowires the series resistances ranges from 1.03 to 3.19 Mohm, comparable to previous measurements of the intrinsic properties of ZnO nanowires,[28] indicating that series resistance is not a significant factor in determining the nature of the *I*−*V* curves in Figure 2; it is dominated by the Au−ZnO junction. To ensure the stability of the contacts, a nanowire was subjected to 45 consecutive *I*−*V* measurements of the Au contact that showed no degradation in the rectifying Schottky-like behavior (see Supporting Information Figure S5). This also showed that self-heating of the nanowire or the interface does not induce any irreversible damage.

Transport Simulations. Full 3D numerical calculations of the electrostatics and transport across the interface as a function of applied bias were performed to explain the experimental results and accurately simulate the complex interplay of finite nanowire and contact geometry (see the structures in Figure 3b). This was performed using the commercial device simulation tool ATLAS by Silvaco.[32]

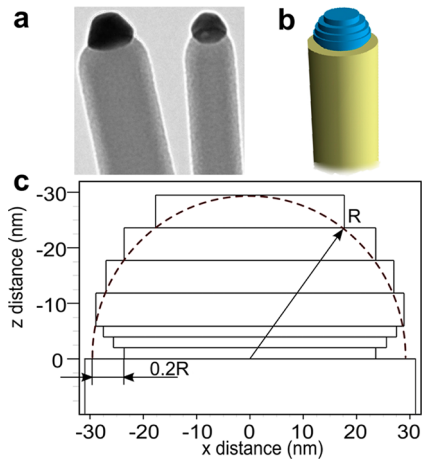

Figure 3. Au contact shape approximated in the simulations. (a) TEM image of the ZnO nanowires with a catalyst particle at the end. (b) 3D model structure of the nanowire and Au particle. (c) Schematic diagram of the geometry used to approximate the Au metal contact and interface geometry in the 3D simulations.

The model replicates a radially symmetric ZnO nanowire approximated as a cylinder with a flat terminating face and a diameter of 75 nm and a length of 900 nm, having an electron affinity[7] of 4.5 eV and n-type doping of 10^{18} cm^{-3}, in accordance with previously measured properties for similarly grown nanowires on sapphire substrate using Au catalyst.[33] At the end of the nanowire, Au contacts with diameters of 40, 50, and 60 nm were considered with a work function of 5.1 eV. The geometry of the Au catalyst particles, shown in Figure 3a, was approximated by a hemisphere of radius *R* (Figure 3b,c). It was observed that the true interface diameter was ~80% of the Au particle diameter and always smaller than the nanowire diameter. In the model, the Au contact is mimicked using

DOI: 10.1021/nl503743t
Nano Lett. 2015, 15, 4248−4254

four large cylinder layers to approximate the hemispherical shape and three smaller cylindrical layers to mimic the shape at the base near the interface (Figure 3c). The second electrical contact, defined as Ohmic, was assumed to be at the base of the nanowire, 900 nm from the Au interface. Transport mechanisms including thermionic emission, recombination, and tunneling across the Schottky barrier at the metal−nanowire interface were all included in the 3D simulations. The thermionic emission current was calculated taking into account the surface recombination velocity, static dipole effects, a field dependent barrier lowering originating from the image force, and band-to-band recombination.[34] Tunneling was considered for both electrons and holes, where localized tunneling rates were calculated through the structure of the semiconductor close to the interface using solutions of Schrödinger equation within the universal Schottky tunneling model (details of the model are in the Supporting Information model description).[35] Although surface-enhanced transport mechanisms such as recombination[15] can play a role in contact behavior for thin nanowires below 50 nm diameter, the transition from Ohmic-like to Schottky-like behavior observed in the ZnO nanowires depends only on R_{Au}. There is no dependence on the absolute nanowire (40−107 nm) or contact (23−71 nm) diameter in the size range measured that would indicate surface-related transport. Therefore, for the materials measured here, surface-enhanced conduction is not considered significant to the transport behavior. In the model, the barrier height is set to 0.6 eV by material parameters using the standard Schottky−Mott theory and is a typical barrier height of vacuum formed Au contacts on ZnO, representative of the clean contacts measured here.[36] The model allows for surface charge to be included on the exposed surface of the nanowire to simulate depletion or accumulation conditions; however, to replicate the experimental $I-V$ measurements, no surface charge was required. The consideration of three transport mechanisms, surface charge, and geometric effects in 3D represents the most comprehensive model to date for calculating transport in nanowire contacts.[5,8,15,37,38]

Discussion. The calculated $I-V$ curves for the bias regime of ±1 V are displayed in Figure 4a for R_{Au} = 0.53 (green), R_{Au} = 0.67 (red), and R_{Au} = 0.80 (blue) for contacts with a diameter of 40, 50, and 60 nm on a 75 nm diameter nanowire. For comparison, experimental results are shown in Figure 4b for a similar range of R_{Au} (0.54, 0.67, and 0.72). Note the agreement in current magnitude and the trend of increasing rectification with increasing R_{Au}; the simulations accurately reproduce the effects observed experimentally, particularly in reverse bias. The simulated $I-V$ characteristics reveal that the reverse bias current density increases when the contact size is decreased, an indication of enhanced tunneling. As the metal particle diminishes in size, tunneling also dominates the forward bias current at a low bias whereas thermionic emission dominates at higher biases. Recombination was found to be negligible due to the large band gap and low intrinsic hole concentration in ZnO. The change in the electrical behavior can be expressed by a rectification ratio, defined as the ratio of forward bias current at +1 V to reverse bias current at −1 V. Figure 4c shows the rectification ratio for 11 contacts determined from the experimental data compared to the simulated rectification ratios. There is a trend of increasing rectification as R_{Au} increases with a transition to Schottky-like behavior at a value of 0.6; below R_{Au} of 0.6, the rectification ratio decreases toward

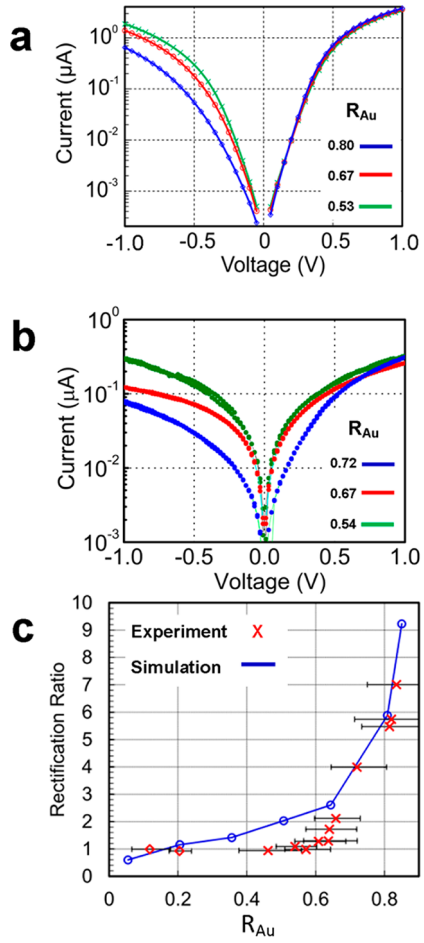

Figure 4. Comparison of the simulation results with the experimental measurements. (a) Simulated $I-V$ characteristics for R_{Au} = 0.53 (green), R_{Au} = 0.67 (red), and R_{Au} = 0.80 (blue). (b) Experimental $I-V$ characteristics for R_{Au} = 0.54 (green), R_{Au} = 0.67 (red), and R_{Au} = 0.72 (blue). (c) Rectification ratio, $I(1\ V)/I(-1\ V)$, for the experimental data (red crosses) as a function of R_{Au} is compared to the simulations (blue circles) (the experimental error bars account for the diameter variation of the hexagonal nanowire and for the ±2 nm measurement error of the Au diameter).

1.0, which defines pure Ohmic behavior. To pinpoint the origin of this effect, the simulated results are examined in more detail.

Previously, Smit et al.[16] predicted that when a metal contact to a semiconductor is reduced in size, spanning the microscale to the nanoscale, a large reduction in depletion width will be observed. However, the Au particle size range considered here is not large enough to bring sufficient change in the depletion width at the center of the contact. Instead, the diminishing size of the contact will produce a depletion region that will narrow near the contact edge as shown by the conduction band profile in Figure 5a. The reduction in depletion width has a profound effect on the tunneling current which is exponentially dependent on the barrier thickness, inducing a larger contribution from tunnel current at the contact edge. This is confirmed by the experimental data and simulations showing increased conductance in reverse bias as the contacts were reduced in size. Figure 5b shows the spatial distribution of current density at the contact edge which is concentrated at the periphery of the interface area. This confirms that tunneling occurs almost exclusively through the narrow depletion region at the edge of the contact. This concentration of current could

DOI: 10.1021/nl503743t
Nano Lett. 2015, 15, 4248−4254

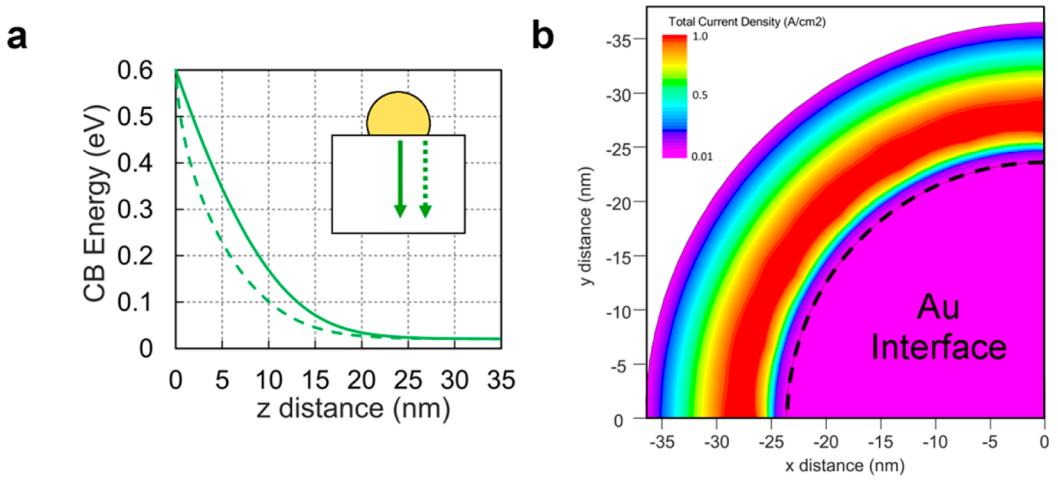

Figure 5. Simulation results depicting the edge effect. (a) Simulated conduction band (relative to the Fermi level) profile along the *z*-axis, down into the nanowire for R_{Au} = 0.53 with a 40 nm diameter contact, at the contact center (solid line), and contact edge (dashed line), as shown by the inset diagram. (b) Plot in the top-down view of the current density on the top face of a nanowire with R_{Au} = 0.80, a 60 nm diameter contact (48 nm interface) at 0.2 V bias. The dashed line indicates the edge of the contact interface.

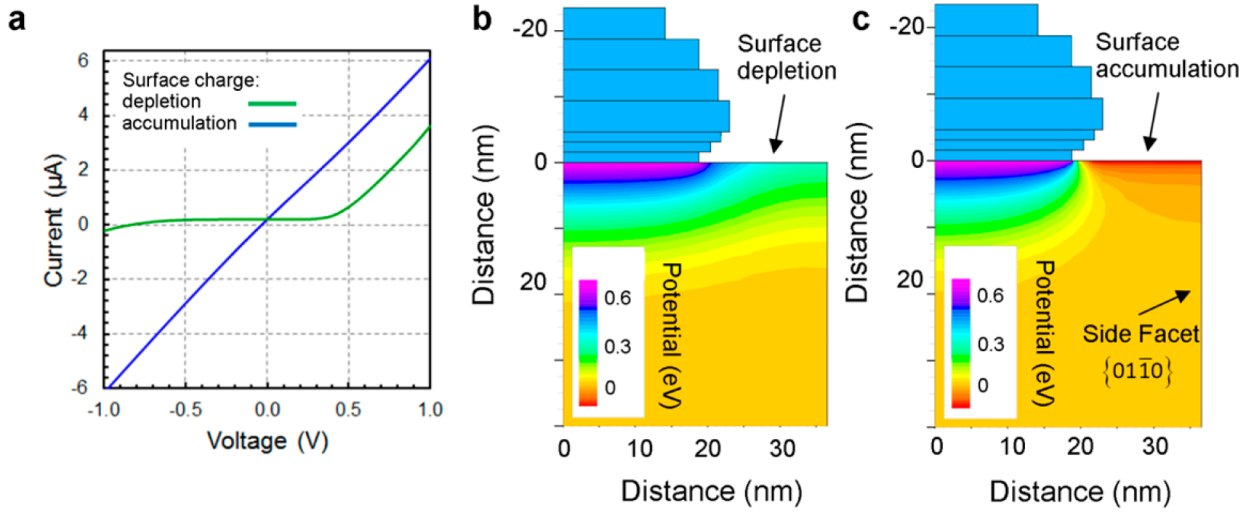

Figure 6. Simulations results depicting the effect of surface charge. (a) Graph shows the simulated *I*−*V* characteristics for a nanowire with R_{Au} = 0.67 and surface charge on the top facet of the nanowire around the Au contact for the following cases: acceptor charge density of 1×10^{12} cm^{-2} (green); donor charge of density 1×10^{13} cm^{-2} (blue). Plots (b) and (c) show the spatial distribution of the conduction band minimum energy (relative to the Fermi level) when there is an acceptor charge density of 1×10^{12} cm^{-2} and donor charge of density 1×10^{13} cm^{-2}, respectively.

lead to local breakdown of the interface due to self-heating. However, we have previously shown[39] that self-heating is negligible for a nanowire contact in the current range measured here; for $R_{Au} \approx 0.5$ (30 nm diameter contact) a rise of ~100 °C is not achieved until the current reaches 10 μA. Additionally, this modest temperature rise is not sufficient for thermionic emission to become comparable to tunneling at low or reverse bias.

The narrowing of the depletion region at the edge is more pronounced for ZnO nanowire contacts due to the complex curved shape of the undercut Au particle, reducing the interface area. To confirm this characteristic, a simple cylindrical metal contact covering the entire end of the nanowire structure with R_{Au} of 1.0 was simulated; such a geometry is typical for Si,[40] Ge,[15] and GaAs[8,41] nanowires. The results reveal Schottky-like behavior as the edge tunneling is negligible, in agreement with the published data for Ge and GaAs nanowires. It is important to stress that only a full 3D model reveals the enhanced edge effect on the transport behavior; 2D models[15,16] underestimate the edge influence on a circular contact (see Supporting Information Figure S6).

Although no surface charge was required to provide agreement between the simulated and experimental results here, the electrostatic condition of the semiconductor surface can affect the transport in nanostructures. This is highly debated for ZnO with many reports showing polar and nonpolar ZnO facets in accumulation, while studies of large-area nanowire arrays show a generalized depletion.[42−44] The effect on the *I*−*V* characteristics of accumulation or depletion of the side and top surfaces of the nanowires is explored through simulations. For example, it is possible to increase the rectification of a Schottky-like contact with R_{Au} = 0.67 when there is a trap density greater than 10^{11} cm^{-3} on the nanowire {01$\bar{1}$0} side facets creating a depletion region. This would be expected because the conduction channel through the wire is reduced in size by the depletion region,[33] which is the

DOI: 10.1021/nl503743t
Nano Lett. 2015, 15, 4248−4254

equivalent of increasing R_{Au} (see Supporting Information Figure S7). However, under accumulation conditions on the nanowire $\{01\bar{1}0\}$ side facets, if R_{Au} is increased above 0.67, the space charge region associated with the contact overlaps with the space charge region of the nanowire surface, inducing more Ohmic-like behavior. The overlap creates a more profound effect when surface charge is present on the nanowire surface surrounding the contact edge.[21] Depletion of the nanowire top facet around the contact periphery leads only to more rectifying behavior (see Figure 6a) regardless of the Au size as the nanowire surface depletion region combines with the contact depletion region, increasing the tunnel path length and "blocking-off" edge tunneling (see Figure 6b). Accumulation of the nanowire top facet leads to more Ohmic-like behavior (Figure 6a) as the edge tunneling is further enhanced by a contact depletion region that is "squeezed in" at the contact periphery (see Figure 6c and Supporting Information Figure S8). These results can be used to explain the experimental findings of other nanowire materials. For example, the inclusion of surface charge confirms that when $R_{Au} \sim 1$ and when the surface is depleted due to adsorbates or a dielectric shell, there is no edge tunneling. This is because the combined depletion region extends far into the wire, as shown by Léonard et al.[15] On the other hand, accumulation of 1×10^{13} cm^{-2} on the nanowire produces Ohmic-like simulation results which is typical for materials such as InAs[14,45] where Au catalyst particle contacts exhibit Ohmic-like behavior. Bulk defects that produce energy states within the bandgap can act as donor- or acceptor-type traps and influence defect-assisted tunneling and recombination. Including recombination due to defects and defect-assisted tunneling in the simulations shows that bulk donor defects produce more Ohmic contacts while bulk acceptor defects increase rectification. However, defects alone cannot replicate the measured Schottky to Ohmic transition, as shown in Supporting Information Figure S9.

In summary, our measurements have thus confirmed the presence of edge tunneling in nanocontacts[4,16] by controlling the tunnel current path around the contact edge. For the results presented here, a transition from Schottky-like to Ohmic-like contact behavior was observed when R_{Au} was less than 0.6. The transition was achieved without engineering the interface other than decreasing the size of the contact relative to the nanowire diameter. Much effort by other groups has been dedicated to finding suitable methodologies to reduce the Schottky barrier height of rectifying end covered contacts, where R_{Au} is 1.0. For example, Suyatin et al. reduced the barrier height of Au nanocontacts on GaAs nanowires to 0.35 eV with the inclusion of a surface dipole layer at the contact interface softening the rectification.[8] Here, the intricacies of the nanowire contact geometry, size, and nanowire surface charge could provide a simple and easily scalable means through which quantum effects can be used to control the transport properties.

Conclusion. A transition between Ohmic-like and Schottky-like Au contact behavior has been measured at the nanoscale and related to the size of the metal contact when compared to the ZnO nanowire diameter. The transition occurs at a contact-to-nanowire diameter ratio of 0.6 due to geometric effects influencing the contact depletion region and leading to enhanced tunneling at the contact periphery. We have shown this dependence for catalytic Au−ZnO nanowire interfaces, free from extraneous structural and chemical issues that could influence transport across the nanoscale junctions; the interfaces formed are of high quality and abrupt, making them suitable for reliable electrical measurements. Furthermore, our full 3D finite-element physically based simulations of realistic nanocontact geometries have confirmed that the observed transition in contact behavior between Ohmic-like and Schottky-like transport is due to enhanced tunneling at the contact edge. If it were possible to select or engineer the ratio of the contact size to nanowire diameter, it would be possible to control the contact type and transport mechanism. The results provide a fundamental understanding of the transport processes surrounding metal contacts to nanowires and also a practical method to fabricate Ohmic or Schottky contacts to nanowires where the interface is abrupt.

■ ASSOCIATED CONTENT

Supporting Information

Additional microscopy, experimental $I-V$, and simulation data; detailed descriptions of the measurement process and model. The Supporting Information is available free of charge on the ACS Publications website at DOI: 10.1021/nl503743t.

■ AUTHOR INFORMATION

Corresponding Author

*E-mail s.p.wilks@swansea.ac.uk.

Present Address

A.S.W.: Interdisciplinary Nanoscience Center (iNano), Aarhus University, Gustav, Wieds Vej 14, DK-8000 Aarhus C, Denmark.

Notes

The authors declare no competing financial interest.

■ ACKNOWLEDGMENTS

HAADF analysis was performed at the SuperSTEM Laboratory, the UK National Facility for Aberration-Corrected STEM, funded by the EPSRC. This work was supported by the Engineering and Physical Sciences Research Council-funded Impact Acceleration Account [grant number EP/K504002/1] and the Royal Society [grant number UF090141]. TEM characterization data was enabled via support from the EPSRC-funded Leeds EPSRC Nanoscience and Nanotechnology Equipment Facility (LENNF) (grant number EP/K023853/1). O.K. thanks Zienkiewicz Scholarship (Swansea University, UK) for the financial support.

■ REFERENCES

(1) Rhoderick, E. H.; Williams, R. H. *Metal-Semiconductor Contacts*; Clarendon Press: Oxford, 1988.
(2) Tung, R. *Phys. Rev. B* **1992**, *45*, 13509−13523.
(3) Sze, S.; Ng, K. *Physics of Semiconductor Devices*; John Wiley and Sons: Hoboken, NJ, 2006.
(4) Qin, W.; Hou, J.; Bonnell, D. A. *Nano Lett.* **2015**, *15*, 211−217.
(5) Léonard, F.; Talin, A. A. *Nat. Nanotechnol.* **2011**, *6*, 773−783.
(6) Chu, S.; Wang, G.; Zhou, W.; Lin, Y.; Chernyak, L.; Zhao, J.; Kong, J.; Li, L.; Ren, J.; Liu, J. *Nat. Nanotechnol.* **2011**, *6*, 506−510.
(7) Wang, Z. L.; Song, J. *Science* **2006**, *312*, 242−246.
(8) Suyatin, D. B.; Jain, V.; Nebol'sin, V. A.; Trägårdh, J.; Messing, M. E.; Wagner, J. B.; Persson, O.; Timm, R.; Mikkelsen, A.; Maximov, I.; Samuelson, L.; Pettersson, H. *Nat. Commun.* **2014**, *5*, 3221.
(9) Song, J. Q.; Ding, T.; Cai, Q. *Appl. Phys. Lett.* **2010**, *96*, 203113.
(10) Carroll, D. L.; Wagner, M.; Rühle, M.; Bonnell, D. A. *Phys. Rev. B* **1997**, *55*, 9792−9799.
(11) Smit, G. D. J.; Rogge, S.; Klapwijk, T. M. *Appl. Phys. Lett.* **2002**, *80*, 2568.

DOI: 10.1021/nl503743t
Nano Lett. 2015, 15, 4248−4254

(12) Park, W. I.; Yi, G.-C. In 2003 Third IEEE Conference on Nanotechnology, Proceedings of IEEE-NANO 2003, 2003; Vol. 2, pp 410−413.
(13) Lord, A. M.; Walton, A. S.; Maffeis, T. G.; Ward, M. B.; Davies, P.; Wilks, S. P. *Nanotechnology* **2014**, *25*, 425706.
(14) Timm, R.; Persson, O.; Engberg, D. L. J.; Fian, A.; Webb, J. L.; Wallentin, J.; Jönsson, A.; Borgström, M. T.; Samuelson, L.; Mikkelsen, A. *Nano Lett.* **2013**, *13*, 5182−5189.
(15) Léonard, F.; Talin, A.; Swartzentruber, B.; Picraux, S. *Phys. Rev. Lett.* **2009**, *102*, 106805.
(16) Smit, G. D. J.; Rogge, S.; Klapwijk, T. M. *Appl. Phys. Lett.* **2002**, *81*, 3852−3854.
(17) Hägglund, C.; Zhdanov, V. P. *Physica E* **2006**, *33*, 296−302.
(18) Lord, A. M.; Ward, M. B.; Evans, J. E.; Davies, P. R.; Smith, N. A.; Maffeis, T. G.; Wilks, S. P. *J. Phys. Chem. C* **2014**, *118*, 21177−21184.
(19) Hou, J.; Nonnenmann, S. S.; Qin, W.; Bonnell, D. A. *Adv. Funct. Mater.* **2014**, *24*, 4113−4118.
(20) Hou, J.; Nonnenmann, S. S.; Qin, W.; Bonnell, D. A. *Appl. Phys. Lett.* **2013**, *103*, 252106.
(21) Yu, A. Y. C.; Snow, E. H. *J. Appl. Phys.* **1968**, *39*, 3008.
(22) Yang, P.; Yan, H.; Mao, S.; Russo, R.; Johnson, J.; Saykally, R.; Morris, N.; Pham, J.; He, R.; Choi, H.-J. *Adv. Funct. Mater.* **2002**, *12*, 323−331.
(23) Barnett, C. J.; Kryvchenkova, O.; Wilson, L. S. J.; Maffeis, T. G. G.; Kalna, K.; Cobley, R. J. *J. Appl. Phys.* **2015**, *117*, 174306.
(24) Cobley, R. J.; Brown, R. A.; Barnett, C. J.; Maffeis, T. G. G.; Penny, M. W. *Appl. Phys. Lett.* **2013**, *102*, 023111.
(25) Allen, J. E.; Hemesath, E. R.; Perea, D. E.; Lensch-Falk, J. L.; LiZ, Y.; Yin, F.; Gass, M. H.; Wang, P.; Bleloch, A. L.; Palmer, R. E.; Lauhon, L. J. *Nat. Nanotechnol.* **2008**, *3*, 168−173.
(26) Bar-Sadan, M.; Barthel, J.; Shtrikman, H.; Houben, L. *Nano Lett.* **2012**, *12*, 2352−2356.
(27) Perea, D. E.; Allen, J. E.; May, S. J.; Wessels, B. W.; Seidman, D. N.; Lauhon, L. J. *Nano Lett.* **2006**, *6*, 181−185.
(28) Lord, A. M.; Maffeis, T. G.; Walton, A. S.; Kepaptsoglou, D. M.; Ramasse, Q. M.; Ward, M. B.; Köble, J.; Wilks, S. P. *Nanotechnology* **2013**, *24*, 435706.
(29) Kirkham, M.; Wang, X.; Wang, Z. L.; Snyder, R. L. *Nanotechnology* **2007**, *18*, 365304.
(30) Brewster, M. M.; Zhou, X.; Lim, S. K.; Gradečak, S. *J. Phys. Chem. Lett.* **2011**, *2*, 586−591.
(31) Mosbacker, H. L.; Zgrabik, C.; Hetzer, M. J.; Swain, A.; Look, D. C.; Cantwell, G.; Zhang, J.; Song, J. J.; Brillson, L. J. *Appl. Phys. Lett.* **2007**, *91*, 072102.
(32) *ATLAS Users Manual*; Silvaco Inc., 2012.
(33) Hong, W.; Sohn, J. I.; Hwang, D.; Kwon, S.-S.; Jo, G.; Song, S.; Kim, S.; Ko, H.-J.; Park, S.-J.; Welland, M. E.; Lee, T. *Nano Lett.* **2008**, *8*, 950−956.
(34) Hurkx, G. A. M.; Klaassen, D. B. M.; Knuvers, M. P. G. *IEEE Trans. Electron Devices* **1992**, *39*, 331−338.
(35) Matsuzawa, K.; Uchida, K.; Nishiyama, A. *IEEE Trans. Electron Devices* **2000**, *47*, 103−108.
(36) Ozgur, U.; Alivov, Y. I.; Liu, C.; Teke, A.; Reshchikov, M. A.; Dogan, S.; Avrutin, V.; Cho, S.-J.; Morkoc, H. *J. Appl. Phys.* **2005**, *98*, 41301.
(37) Hu, J.; Liu, Y.; Ning, C. Z.; Dutton, R.; Kang, S.-M. *Appl. Phys. Lett.* **2008**, *92*, 083503.
(38) Bussone, G.; Schäfer-Eberwein, H.; Dimakis, E.; Biermanns, A.; Carbone, D.; Tahraoui, A.; Geelhaar, L.; Haring Bolívar, P.; Schülli, T. U.; Pietsch, U. *Nano Lett.* **2015**, *15*, 981−989.
(39) Kryvchenkova, O.; Kalna, K.; Cobley, R. J. In 10th International Conference on Advanced Semiconductor Devices & Microsystems (ASDAM), 2014; pp 1−4.
(40) Kodambaka, S.; Tersoff, J.; Reuter, M. C.; Ross, F. M. *Phys. Rev. Lett.* **2006**, *96*, 096105.
(41) Korte, S.; Steidl, M.; Prost, W.; Cherepanov, V.; Voigtländer, B.; Zhao, W.; Kleinschmidt, P.; Hannappel, T. *Appl. Phys. Lett.* **2013**, *103*, 143104.
(42) Heinhold, R.; Williams, G. T.; Cooil, S. P.; Evans, D. A.; Allen, M. W. *Phys. Rev. B* **2013**, *88*, 235315.
(43) Heinhold, R.; Cooil, S. P.; Evans, D. A.; Allen, M. W. *J. Phys. Chem. C* **2014**, *118*, 24575−24582.
(44) Lord, A. M.; Maffeis, T. G.; Allen, M. W.; Morgan, D.; Davies, P. R.; Jones, D. R.; Evans, J. E.; Smith, N. A.; Wilks, S. P. *Appl. Surf. Sci.* **2014**, *320*, 664−669.
(45) Durand, C.; Berthe, M.; Makoudi, Y.; Nys, J.-P.; Leturcq, R.; Caroff, P.; Grandidier, B. *Nanotechnology* **2013**, *24*, 275706.

DOI: 10.1021/nl503743t
Nano Lett. 2015, 15, 4248−4254